



Al-Khwarizmi Engineering Journal ISSN (printed): 1818 – 1171, ISSN (online): 2312 – 0789 Vol. 21, No. 4, December, (2025), pp. 93- 105

Analysing the Effects of Switching, Conduction and Thermal Losses on IGBT Performance in Boost DC–DC Converters for Photovoltaic Systems

Muhanad D. Hashim Almawlawe

Department of Electronics and communication Engineering ,College of Engineering, University of Al-Qadisiyah, Al-Qadisiyah, Iraq

Email: muhanad.almawlawe@qu.edu.iq

(Received 9 April 2025; Revised 13 September 2025; Accepted 19 October 2025; Published 1 December 2025) https://doi.org/10.22153/kej.2025.10.003

Abstract

This study examines the thermal and electrical characteristics of insulated gate bipolar transistors (IGBTs) in boost direct current (DC)–DC converters used in photovoltaic systems with respect to how switching and conduction losses vary under different operating conditions. The behaviour of IKWH70N65WR6 IGBT was measured (PLECS software) with load resistances of 5, 10 and 20 Ω at switching frequencies of 1–100 kHz. Important results are as follows: conduction losses prevail at low frequencies and load currents and switching losses increase towards high frequencies. Thermal stress is the highest at mid-range frequencies (50–60 kHz) and IGBT junction temperatures peak to 123 °C. Reduced load resistance leads to increased power consumption and total losses, and the value of load matching must be optimised. This study offers critical data regarding the choice and optimisation of IGBTs to improve efficiency and reliability within the uses of renewable energies.

Keywords: IGBT losses; step-up DC–DC converter; photovoltaic systems; conduction losses; switching losses; thermal control; efficiency optimisation; continuous conduction mode (CCM)

1. Introduction

Renewable energy systems have been used extensively in the recent years as a sustainable substitute to power generation based on fossil fuels, which is linked to the high rate of environmental degradation [1][2]. Amongst these systems, photovoltaic (PV) systems utilise the power of the sun and transform it into direct current (DC) voltage by using a number of subsystems. However, the power emitted by solar panels is typically too low and cannot be used directly to charge a battery or be linked to a grid. Thus, a voltage-boosting stage is necessary.

A boost DC–DC converter is widely used in PV systems to raise low panel voltage to a level required

by other downstream systems (e.g. battery storage or grid-tied inverters) [3]-[5]. This converter consists of important elements, such as an inductor; a capacitor; a semiconductor switch, typically a metal—oxide—semiconductor field-effect transistor (MOSFET) or an insulated gate bipolar transistor (IGBT); and a diode. The synchronised switching behaviour of this converter, which is controlled by the duty cycle, allows increasing the voltage.

The assumptions used in the current study are operation in continuous conduction mode (CCM), input voltage ($V_{\rm in}$) of 48 V, output voltage ($V_{\rm out}$) of 100 V, switching frequency of 1–100 kHz and load resistance of 5–20 Ω . The efficiency of the target is approximately 90%.

This is an open access article under the CC BY license:



The primary motivation of the current study arises from the critical need to enhance the efficiency, reliability and thermal robustness of boost DC–DC converters used in PV systems.

1.1 Literature Review

In this section, a literature review highlights the relationship between the losses of the switching components and the improvement in efficiency of the step-up converter [6]- [10].

These previous studies are considered under different environmental conditions with various control strategies and authors' overviews. They focus on the characteristics of IGBTs and diodes from the following views.

1.1.1 Importance of Loss Minimisation in Power Electronics

One of the grounds for enhancing the effectiveness of step-up DC-DC converters is loss minimisation. Esram and Chapman in [3] reported that the effectiveness of maximum power point tracking (MPPT) techniques in PV systems is closely related to the performance of converters, which, in turn, is dependent on converter losses. Efficiency has been pursued with the incorporation of high materials with less loss coefficients, including gallium nitride (GaN)-based devices Graditi et al. in [8] established that GaN-based synchronous rectifiers could significantly lower switching loss in power factor correction boost converters a path towards provide greater efficiency. Almawlawe et al. in [2] used digital converters in low-switching-loss solar panel converters; this technique not only provided an innovation for control strategies but was also the key to minimising switching losses. The aforementioned developments highlight the importance of an overall loss analysis, for conduction and switching losses, with the aim of maximising the performance of a system.

1.1.2 Thermal Management Challenges

The problem of heat dissipation is challenging as far as the stable functioning and reliability of IGBTs in high-frequency converters are concerned. The approach to thermal management in power electronics was defined broadly by Rahman et al. in [10] to highlight the effect of losses on the temperature of devices and their dependence on temperature. At high junction temperatures, a threat of thermal stress exists, shortening the life of components, such as diodes and IGBTs. The

reviewed articles examined the dependence of switching frequency, heat sink temperature and junction temperatures on load resistance (R = 5, 10 and 20 Ω). For example, when R = 5 Ω and f = 100 kHz, IGBT junction temperatures reach approximately 118 °C. Meanwhile, they reach approximately 88 °C when R = 20 Ω . These results are consistent with the findings in Chaithanakulwat [9], who underlined the significance of higherfficiency power conversion in renewable power sources to reduce thermal adversities.

1.1.3 Efficiency Optimisation Techniques

The optimisation of the efficiency of step-up DC-DC converters comprise a set of high-level control algorithms, topology redesigning and novel materials. Sullivan and Zhang in [11] suggested the simplified design of a litz wire that minimised alternating current (AC) losses in inductors, enhancing total efficiency. Similarly, the design and use of transformers and inductors in power electronics were discussed by Hurley and Wölfle [12], with emphasis on core loss modelling via the Steinmetz equation. Trade-offs between switching frequency and efficiency were also marked in the reviewed papers. Although operation at very high frequencies (>100 kHz) lowers thermal stress, it causes the difficulty of more switching losses. Zhang and Peng in [8] performed a step-by-step loss analysis and optimisation of DC-DC converters on PV applications, offering guidelines in the practical selection of components and component working parameters.

1.1.4 Control Strategies for Dynamic Performance

In boost DC-DC converters, advanced control methods are important for suppressing losses and improving dynamic performance. The implementation of a boost converter with quasisliding mode control presented by TRUJILLO, Simeón Casanova [13] was demonstrated to achieve better transient response and stability because of microcontroller-based its implementation. Hawsawi in [5] discussed switched capacitor boost converters to incorporate solar PV, with particular interest in augmenting MPPT dynamically. Future research programmes will involve developing adaptive gate-drive methods and real-time control programmes to allow converter operation to be adjusted dynamically changing conditions. to load Strategies will be developed to solve the highfrequency operation problems and guarantee optimum performance over a significant operating range.

1.1.5 Comparison of Component Characteristics

The performance of IGBTs and diodes in step-up converters is strongly influenced by their switching and conduction characteristics. The reviewed papers provide extensive data on IGBT and diode losses under varying frequencies and load resistances. For example,

IBGT losses = 28.99 W, diode losses = 31.44 W when $R = 5 \Omega$ and f = 10 kHz.

• $R=20~\Omega~100~kHz$, loss in IGBT is 13.27 W and that in diodes is 7.19 W. Such findings coincide with those of [14], who conducted research on interleaved zero voltage-switching converters to reduce ripple currents and enhance efficiency. The data underscore the importance of selecting components with optimal characteristics for specific applications.

1.1.6 Renewable Energy Applications

The incorporation of boost DC–DC converters into renewable energy systems, particularly PV systems, requires appropriate attention on efficiency, reliability and cost. Twidell in [1] explained the role of power electronics in renewable energy design, and the necessity of converters with high efficiency to obtain the maximum energy harvest. Singh in [4] identified the relevance of converter design in attaining optimal performance. Chaithanakulwat in [9] conducted an extensive review of high-efficiency power conversion into renewable energy systems, providing knowledge of state-of-the-art methods for addressing loss reduction. All the aforementioned studies support the necessity to maximise the performance of IGBTs in PV-integrated systems. Reference [15] discussed the losses in DC-DC converters and the techniques for improving efficiency by minimising losses. Different techniques for reducing losses in high-frequency DC-DC converters were discussed in [19], [20], [21], including the use of advanced MOSFETs and optimised circuit designs.

1.1.7 Major calculations Used to Design the Set-up Converter

Working in CCM must satisfy the following equation:

$$D_{cycle} = 1 - \frac{V_{in}}{V_{out}}.$$
 ...(1)

The inductor ripple current (ΔI_L) should be less than two times the average inductor current (I_L) .

$$L_{value} = \frac{V_{in} * D_{cycle}}{f_{swit.} * \Delta I_L}, \qquad \dots (2)$$

$$C_{value} = \frac{I_{out} * D_{cycle}}{f_{swit.} * \Delta V_{out}}, \qquad ...(3)$$

where L_{value} is the inductance value, C_{value} is the capacitance value, V_{in} is the input voltage, V_{out} is the output voltage, D_{cycle} is the duty cycle, f_{swit} is the switching frequency, ΔI_L is the inductor ripple current and ΔV_{out} is the output ripple voltage.

The basic scheme for the step-up DC–DC converter is depicted in Figure 1 [6].

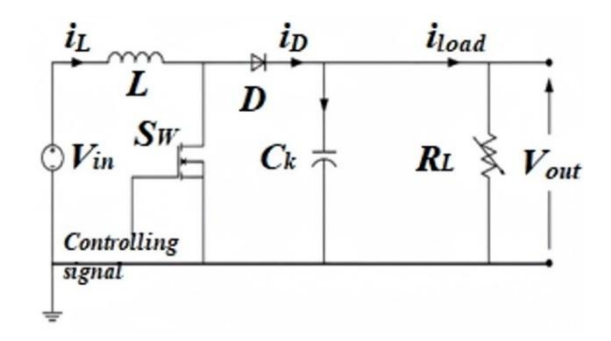


Fig. 1. Basic step-up DC-DC converter scheme.

Moreover, the step-up converter contains switches of the MOSFET or IGBT type and diodes, on which the principle of switching depends on the process of raising or lowering voltages (depending on duty cycle D_{cycle}).

Each of these elements contributes to different types of losses.

- 1) **Switching losses:** They occur during the transition states of a MOSFET, wherein energy is lost due to the finite time it takes for the switch to turn on or off [2].
- 2) **Conduction losses:** They are resistive losses in the switch, diode and inductor windings; they can increase with current and are influenced by the resistance of these components [9].
- 3) **Core Losses:** Losses in the inductor due to hysteresis and eddy currents within the magnetic core material [11].

Enhancing the efficiency of boost converters can be achieved by optimising the properties of the aforementioned components, using sophisticated control methods and by redesigning even converter topology in some cases. Techniques, such as soft switching, synchronous rectification and the use of materials with low loss coefficients, have been explored and implemented to push efficiency boundaries and minimise losses under varying load conditions [11] [12] [16]-[18],. Finally, a table that classifies the aforementioned prior studies summarises the literature review.

Year	Author	Technology Employed	Contribution
2022	Shi and Li	ANN with particle swarm Optimisation (PSO)	Privacy- focused IDS for WSNs; PSO-enhanced ANN performance.
2023	Belarbi et al.	Federated deep learning	Privacy- preserving IDS for IoT that uses federated learning. High-accuracy IDS that
	Gueriani et al.	Hybrid CNN-LSTM	captures spatiotemporal features in IoT traffic.
2024	Shen et al.	Federated learning with ensemble knowledge distillation (FLEKD)	Enhanced IDS performance that addresses data heterogeneity Hybrid IDS
2024	Gowdhaman and Dhanapal	ResNet- Inception + SVM	that achieves 99.46% accuracy on .NSL-KDD

2. Mathematical Model

The theoretical part can be strengthened if a clear connection between component physics and the observed simulation results is established through mathematical modelling. The total losses for the step-up converter working in CCM mode is

$$\begin{split} P_{loss.total} &= P_{lcond.IGBT} + P_{swit.IGBT} \\ &+ P_{lcond.diode} \\ &+ P_{lswit.diode} + P_{L}. \end{split} \tag{4}$$

2.1 IGBT Conduction Losses

$$P_{cond.IGBT} = V_{ceo} * I_{c.avg.} + r_{ce} *$$

$$* I^{2}_{c.rms}, \qquad ...(5)$$

where $P_{cond,IGBT}$ is the conduction power loss in IGBT (W), V_{ce0} is the IGBT threshold voltage (typically 0.7–1.5 V for IGBTs) (V), $I_{c,avg.}$ is the average collector current during the conduction period (A), r_{ce} is the on-state resistance of the IGBT $[\Omega]$, $I_{c,rms}$ is the root mean square (RMS) value of the collector current during the conduction period (A).

For a step-up converter working in CCM mode, previous currents can be calculated as

$$I_{c.avg.} = I_{L.avg.} * D,$$

$$I_{c.rms} = I_{L.rms} * \sqrt{D},$$
...(6)

where $I_{c,avg.}$ is the average inductor current (A), $I_{L.avg.} = \frac{P_{out}}{V_{in}*\gamma} = \frac{V_{out}*I_{out}}{V_{in}*\gamma}$, $I_{L,\mathrm{rms}}$ is the RMS inductor current (A) and $I_{L,rms} = \sqrt{I_{L.avg.}^2 + \frac{\Delta I_L^2}{12}}$.

2.2 IGBT Switching Losses

$$P_{swit,IGBT} = f_{swit} * (E_{ON} + E_{OFF}), \qquad ...(7)$$

where $P_{swit,IGBT}$ is the switching power loss in the IGBT (W), f_{swit} is the switching frequency (Hz), E_{ON} - is the energy loss during the turn-on state (J) and E_{OFF} is the energy loss during the turn-off state [J].

These energy losses can be further modeled as

$$E_{ON} = \int_{0}^{t_{OFF}} v_{ce}(t) * i_{c}(t) dt,$$

$$E_{OFF} = \int_{0}^{t_{ON}} v_{ce}(t) * i_{c}(t) dt.$$
...(8)

These equations can be approximated using datasheet values that are scaled to actual operating conditions:

conditions:
$$E_{ON} = E_{ON.ref} * \frac{V_{ce}}{V_{ce.ref}} * \frac{I_c}{I_{c.ref}} * \frac{I_c}{I_{c.ref}} * \frac{1}{I_{c.ref}} * \frac{1}{I_{c.ref}} * \frac{V_{ce}}{V_{ce.ref}} * \frac{I_c}{I_{c.ref}} * \frac{V_{ce}}{I_{c.ref}} * \frac{I_c}{I_{c.ref}} * \frac{1}{I_{c.ref}} * \frac{1}{$$

where $E_{ON,ref}$ and $E_{OFF,ref}$ are the turn-on and turn-off energy losses under reference conditions (J), $V_{ce,ref}$ is the reference collector-emitter voltage (V), $I_{c,ref}$ is the reference collector current (A), $T_{j,ref}$ is the reference junction temperature (°C), T_c is the temperature coefficient (typically 0.003–0.005 per °C) and T_j is the actual junction temperature (°C).

2.3 Diode Conduction Losses

$$P_{cond.diode} = V_{FO} * I_{F.avg} + r_F * I_{F.rms}^2, \quad ...(10)$$

where $P_{cond.,diode}$ is the conduction power loss in the diode (W), V_{FO} is the diode threshold voltage (typically 0.7–1.0 V) (V), r_F is the on-state resistance of the diode (Ω), $I_{F.avg}$ is the average forward current through the diode (A) and $I_{F,rms}$ is the RMS value of the forward current (A).

For a step-up converter working in CCM mode,

$$I_{F.avg.} = I_{out} = \frac{V_{out}}{R_{load}}; I_{F.rms} = I_{out} *$$

$$\sqrt{\frac{1}{1-D}}. \qquad ...(11)$$

2.4 Diode Switching Losses

$$P_{\text{swit.diode}} = f_{\text{swit}} * E_{rr}, \qquad \dots (12)$$

where $P_{swit.,diode}$ is the switching power loss in the diode (W), and E_{rr} is the reverse recovery energy (J).

The reverse recovery energy can be calculated as

$$E_{rr} = \frac{1}{4} * Q_{rr} * V_R \left[1 + T_{C.rr} \left(T_j - T_{j.ref} \right) \right], \quad \dots (13)$$

where Q_{rr} is the reverse recovery charge (C), V_R is the reverse voltage across the diode during switching (V) and $T_{C,rr}$ is the temperature coefficient for reverse recovery (typically 0.005–0.006 per °C).

2.5 Inductor Losses

$$P_{L} = P_{L.DC} + P_{L.AC}$$

= $I_{L.rms}^{2} * R_{DC} + P_{core}$, ...(14)

where P_L is the total inductor power loss (W); $P_{L,DC}$ is the DC copper loss (W); $P_{L,AC}$ is the AC loss, which is primarily the core loss (W); and R_{DC} is the DC resistance of the inductor winding (Ω).

Core losses can be estimated using the Steinmetz equation:

$$P_{core} = k * f_{swit}^{\alpha} * B_{pk}^{\beta} * V_{core}, \qquad \dots (15)$$

where k, α, β are material-specific Steinmetz parameters, B_{pk} is the peak magnetic flux density (T) and V_{core} is the volume of the magnetic core (m³).

3. Simulation Process

The simulation process was completed using Figure 2, PLECS software and detailed data on switching and conduction losses for an IGBT device, specifically the IKWH70N65WR6 model. Various scenarios are divided into different resistance values (R = 5, 10 and 20 Ω) and various frequencies that range from 1 kHz to 100 kHz.

All electrothermal runs were executed in PLECS 4.6 on a 1 μ s fixed-step solver. Conduction and switching losses were computed internally from device characteristics, whilst thermal quantities were obtained with the built-in 'thermal library' by using Foster coefficient networks.

- **IGBT**: Infineon IKWH70N65WR6 (650 V, 70 A at 25 °C, Tj max 175 °C)
- **Boost diode**: Infineon IDW75E65D1 (650 V, 75 A)
- Inductor: 220 μ H, Kool-M μ 60 μ toroid, 14 turns 2 mm \times 0.8 mm litz wire, measured RDC = 28 m Ω
- Output capacitor: $470 \,\mu\text{F}/250 \,\text{V}$ E-cap, ESR = $110 \,\text{m}\Omega$ @ $20 \,^{\circ}\text{C}$, $100 \,\text{kHz}$
- Heat sink: RthSA = 1.8 K/W (extruded AL 150 mm length, 3 mm fin, natural convection 2 m/s);
 TIM RthCS = 0.35 K/W
- **Ideal gate drive** (no overshoot/undershoot); the measured switching energies already include 15% extra margin for layout inductance (estimated 15 nH).

3.1 Junction Temperature Losses

• For $R = 5 \Omega$ and frequencies of 1-100 kHz

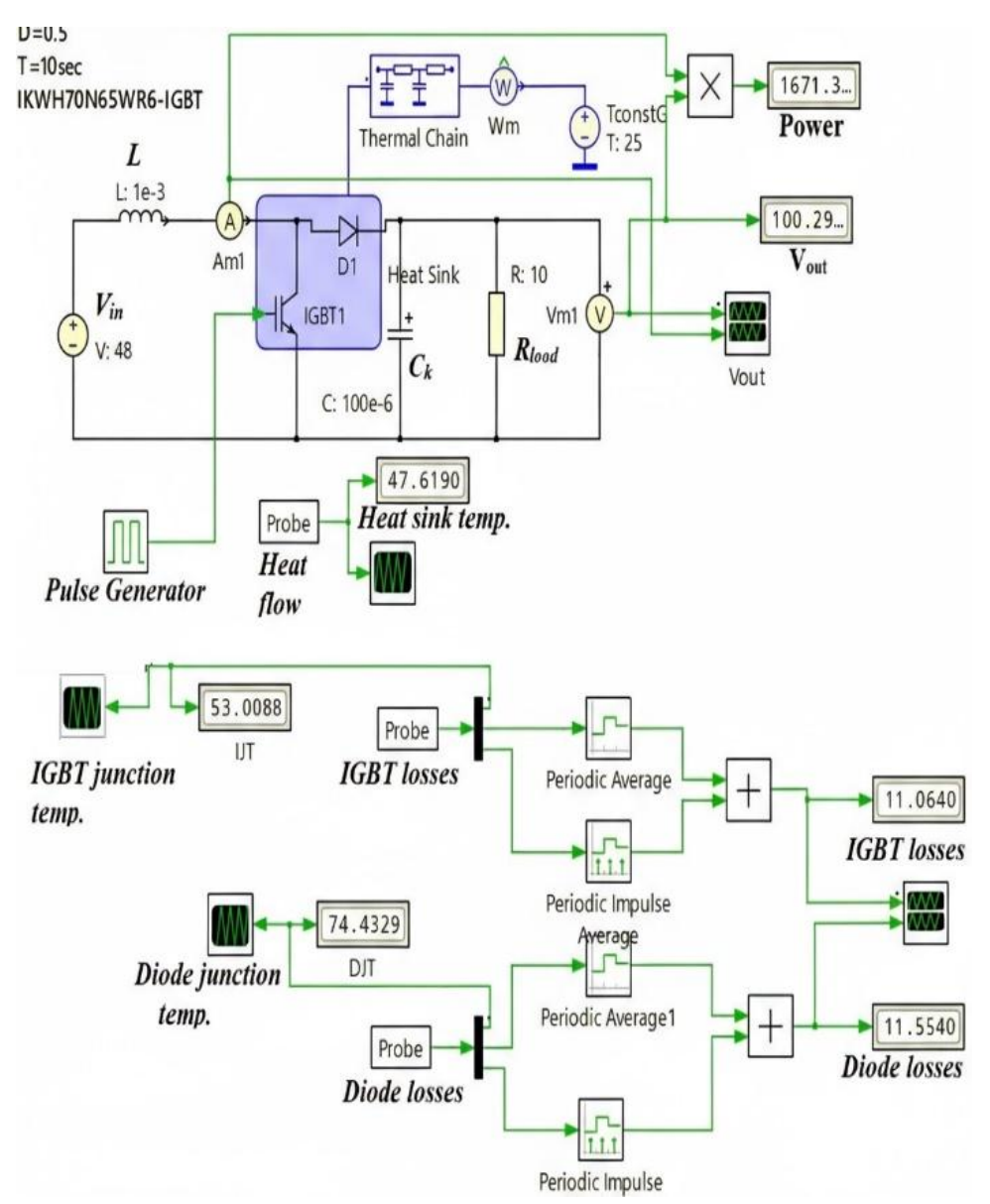


Fig. 2. Circuit of the setup DC-DC converter.

Table 1, $Temperature\ losses\ at\ R_{load}=5\ \Omega$

Temperature losses at Rioad = 3 22				
Frequency	Heat sink temperature	Diode junction	IGBT junction	
(kHz)		temperature	temperature	
1	69.5141	134.3826	77.1753	
5	82.1744	150.5209	95.1672	
10	85.4309	151.4186	99.9818	
50	99.4328		122.9279	
60	96.5419		122.0881	
100	84.6633		118.2692	

• For $R = 10 \Omega$ and frequencies of 1–100 kHz

Table 2, $Temperature \ losses \ at \ R_{load} = 10 \ \Omega$

Frequency (kHz)	Heat sink temperature	Diode junction temperature	IGBT junction temperature
1	44.4157	68.7946	47.8958
5	47.619	73.4129	53.0108
10	48.8675	73.6855	54.9149
50	58.5155	86.4866	68.4873
60	61.0306	90.2099	71.9595
100	71.5927	106.3471	86.4659

• For $R = 20 \Omega$ and frequencies of 1–100 kHz

Table 3, Temperature losses at $R_{load} = 20 \Omega$

Frequency (kHz)	Heat sink temperature	Diode junction temperature	IGBT junction temperature
1	36.9866	47.4033	39.5024
5	34.7991	45.7058	37.1773
10	35.3559	45.8791	38.0362
50	39.756	51.4332	44.3082
60	40.8781	53.0029	45.8885
100	45.4653	59.5084	52.3223
200	57.69	77.5262	69.3008
300	71.1633	98.3546	87.7596

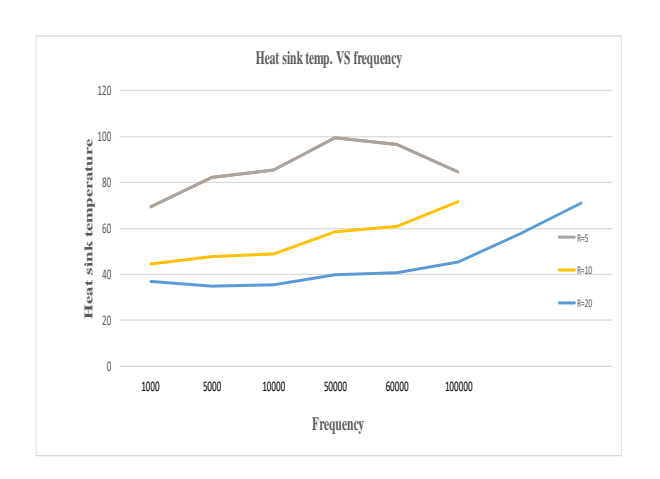


Fig. 3. Heat sink temperature losses vs. frequency.

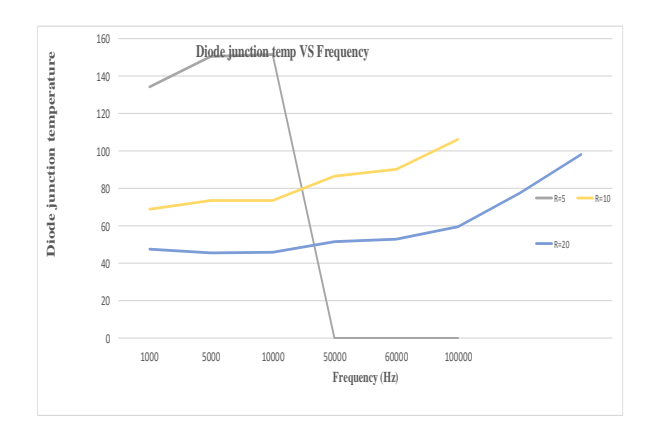


Fig. 4. Diode junction temperature losses vs. frequency.

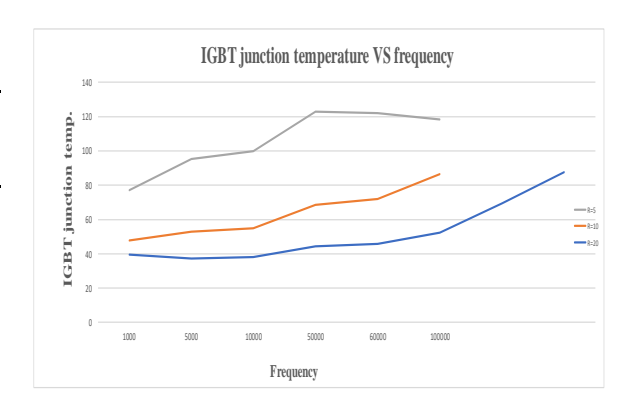


Fig. 5. IGBT junction temperature losses vs. frequency.

Figures 3, 4 and 5 likely present a comparative graph that shows temperature measurements across three components (IGBT junction, diode junction and heat sink) at different switching frequencies. This figure depicts the critical thermal operating points for each component, highlighting that different elements in the converter reach their maximum temperatures at different frequencies. From this figure, we can conclude that the curves likely exhibit rising temperatures as frequency increases, peaking at around 50-60 kHz, followed by a decay at extremely high frequencies. Moreover, the IGBT junction temperatures are the highest (reaching ~123 °C at 50 kHz with $R = 5 \Omega$), followed by diode junction temperatures (reaching ~151 °C at 10 kHz with $R = 5 \Omega$), with heat sink temperatures presenting lower values but similar trends.

3.2 Switching and Conduction Losses

• For $R = 5 \Omega$ and frequencies of 1–100 kHz

Table 4, Switching losses at $R_{load} = 5 \Omega$

Frequency	IGBT	Diode	Power
(kHz)	looses	looses	
1	19.176	25.3391	2178.6038
5	26.7407	30.437	3733.7786
10	28.9968	31.4379	3733.3485
50			3699.3581
60			3697.3194
100			3693.0962

• For $R = 10 \Omega$ and frequencies of 1–100 kHz

Table 5, Switching losses at $R_{load} = 10 \Omega$

Frequency	IGBT	Diode	Power
(kHz)	looses	looses	
1	8.6257	10.7904	424.8729
5	11.064	11.5559	1671.302
10	12.024	11.8445	1765.6378
50	19.3185	14.1989	1829.0381
60	21.1788	14.854	1831.4453
100	28.8015	17.7949	1836.2035

• For $R = 20 \Omega$ and frequencies of 1–100 kHz

Table 6, Switching losses at $R_{load} = 20 \Omega$

Frequency	IGBT	Diode	Power
(kHz)	looses	looses	
1	6.1994	5.788	
5	4.8705	4.9289	699.3105
10	5.3224	5.0338	814.0819
50	8.8221	5.9346	900.7073
60	9.7048	6.174	904.2111
100	13.2742	7.1922	911.1927

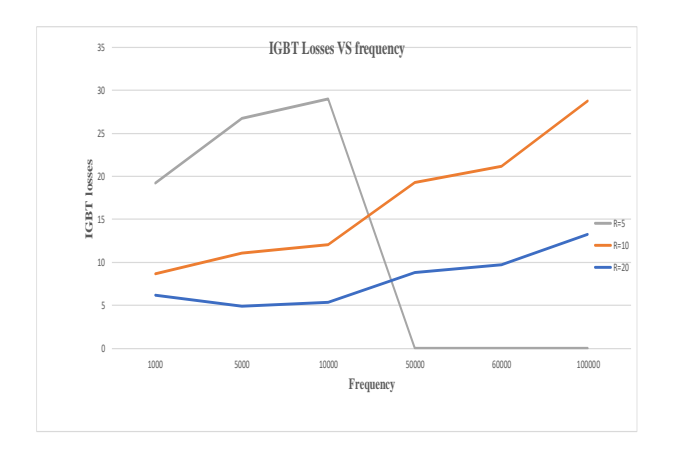


Fig. 6. IGBT switching and conduction losses.

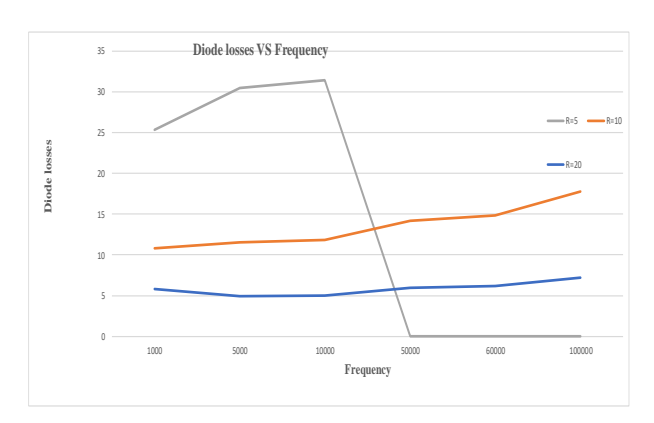


Fig. 7. Diode switching and conduction losses.

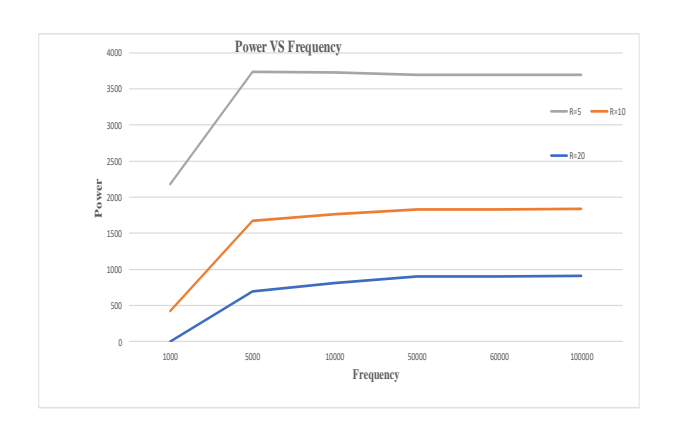


Fig. 8. Dissipated power.

Figures 6, 7 and 8 present the breakdown of power losses between switching and conduction losses for the IGBT and diode components. From this figure, we conclude the following:

- Conduction losses dominate at lower frequencies.
- Switching losses become more significant at higher frequencies.
- Total losses peak at mid-range frequencies (IGBT losses of ~29 W and diode losses of ~31 W at 50 kHz with $R = 5 \Omega$).
- Lower resistance values demonstrate significantly higher losses than higher resistance values.

Figure 6 illustrates the trade-off between conduction and switching losses across different operating frequencies, explaining why thermal performance peaks at mid-range frequencies.

3.3 Heat Sink and Diode Temperature Losses

• For $R = 5-20 \Omega$ and frequencies of 1-100 kHz.

Heat sink temperature at $R_{load} = 5-20 \Omega$

Frequency	At R = 5	At R = 10	At R = 20
(kHz)	Ω	Ω	Ω
1	69.5141	44.4157	36.9866
5	82.1744	47.619	34.7991
10	85.4309	48.8675	35.3559
50	99.4328	58.5155	39.756
60	96.5419	61.0306	40.8781
100	84.6633	71.5927	45.4653



Fig. 9. Heat sink temperature losses vs. frequency and resistance value.

Figure 9 focuses on the heat sink temperature of IGBT behaviour across the full range of investigated frequencies. This figure illustrates how load resistance dramatically affects thermal stress on the heat sink of IGBT, with lower resistance (higher current) conditions creating significantly more challenging thermal control requirements.

Meanwhile, Figure 10 specifically emphasises diode temperature behaviour across different frequencies. This figure indicates that the diode exhibits varying thermal stress distributions under various frequencies than under IGBT, and the highest temperatures in the diode are at different frequencies. This finding implies that thermal control policies must consider the individual behavioral patterns of the components.

Table 8, Diode temperature at $R_{load} = 5 \text{--} 20~\Omega$

Frequency	At R = 5	At R = 10	At R = 20
(kHz)	Ω	Ω	Ω
1	134.3826	68.7946	47.4033
5	150.5209	73.4129	45.7058
10	151.4186	73.6855	45.8791
50		86.4866	51.4332
60		90.2099	53.0029
100		106.3471	59.5084

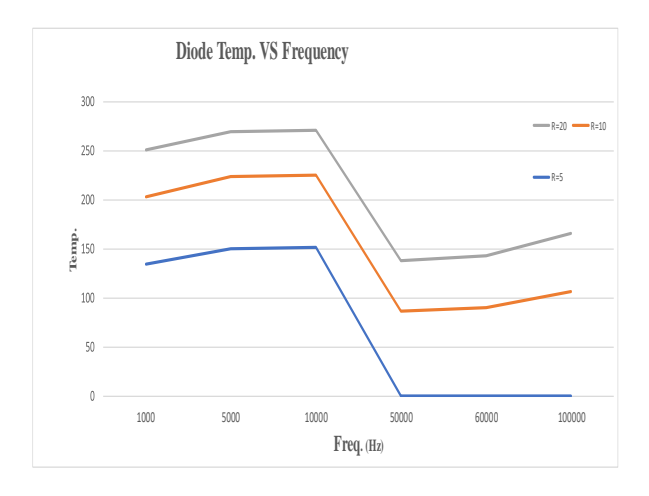


Fig. 10. Diode temperature losses vs. frequency and resistance value.

4. Results and Discussion

4.1 Heat Sink Temperature

- The temperature of a heat sink tends to rise with frequency to a given frequency but tends to decline at extremely high frequencies (e.g. 100 kHz and higher).
- When R = 5 Ω , the highest temperature of the heat sink was recorded as 50 kHz (99.4328 °C). Then, temperature decreased slightly at higher frequencies.
- Similar tendencies were noted in the cases of R = $10~\Omega$ and $20~\Omega$, where temperature was the highest at 50–60 kHz and then reduced.

4.2 Diode Junction Temperature

- Diode junction temperature also rises with increasing frequency, peaking between 50 kHz and 60 kHz.
- For $R = 5 \Omega$, the peak diode junction temperature reached 151.4186 °C at 10 kHz, which remained relatively stable until 50 kHz before becoming unavailable ('-').
- At R = 10 Ω , the diode junction temperature continued to rise even at higher frequencies, reaching 106.3471 °C at 100 kHz.
- For R = 20 Ω , diode junction temperature increased steadily, reaching 98.3546 °C at 300 kHz.

4.3 IGBT Junction Temperature

• The IGBT junction temperature exhibited similar trends as the heat sink and diode junction temperatures.

- Notably, at $R = 5 \Omega$, IGBT junction temperature peaked at 122.9279 °C at 50 kHz.
- For R = 10 Ω and 20 Ω , IGBT junction temperatures were lower but still exhibited peaks at around 50–60 kHz.

4.4 IGBT and Diode Losses

- IGBT and diode losses increase with frequency, reflecting higher switching losses at higher frequencies.
- For example, at $R = 5 \Omega$ and 50 kHz, IGBT losses were 28.9968 W, and diode losses were 31.4379 W.
- At R = 10 Ω , losses were considerably lower compared with R = 5 Ω , particularly at higher frequencies.
- At R = 20 Ω , IGBT and diode losses were the lowest among the three resistance values.

4.5 Power Consumption

- For power consumption, the losses exhibit a similar trend, peaking to a maximum of 50–60 kHz at all resistance values.
- With $R = 5 \Omega$, the maximum power consumption was 3733.7786 W at 5 kHz, which remained relatively constant until 100 kHz.
- At $R=10~\Omega$, power consumption was considerably lower, with the maximum power consumption of 1836.2035 W at 100 kHz.
- At R = $20~\Omega$, power consumption was the minimum, with a value of 911.1927 W at a frequency of 100 kHz.

On the basis of the above information analysed in the context of losses based on switching frequency, we can infer dependable and pegged efficient operation under different circumstances.

- 1) Thermal management: Effective thermal control is crucial, mostly at mid-range frequencies (50–60 kHz), where heat sink and junction temperatures peak.
- 2) **Efficiency:** Lower resistance values (e.g. R = 5 Ω) result in higher power consumption and losses, suggesting less efficient operation compared with higher resistance values (e.g. $R = 20 \Omega$).
- 3) **Frequency dependence:** Operating at very high frequencies (>100 kHz) might lead to reduced thermal stress but could introduce other challenges related to switching losses and overall system efficiency.

5. Conclusions

This work was a systematic research on the thermal and electrical characteristics of IGBTs in boost DC–DC converters to PV systems at different switching frequencies (1-100 kHz) and load resistances (5 Ω , 10 Ω , 20 Ω). The key findings are as follows:

1. Loss mechanisms

- **Conduction losses.** They dominate at low frequencies and high load currents.
- **Switching losses.** As switching frequency increases, energy lost during switching becomes more prominent, reaching its highest point within the 50–60 kHz range.

2. Thermal performance

- **IGBT junction temperatures.** They peak at 123 °C (R = 5 Ω , 50 kHz), whilst **diode junctions** reach 151 °C (R = 5 Ω , 10 kHz).
- **Heat sink temperatures.** The shared patterns in the data highlight the importance of a well-designed cooling system.

3. Efficiency trade-offs

Using a smaller resistor (e.g. 5 Ω) results in more wasted energy (approximately 3.7 kW) and lower overall efficiency. Meanwhile, a larger resistor (e.g. 20 Ω) reduces this energy waste, but its use must be carefully coordinated with the operating frequency to maintain good balance amongst different types of energy loss.

4. Design implications

- Optimal frequency ranges (≈20–50 kHz) exist to minimise total losses whilst maintaining thermal limits.
- Component selection (e.g. IGBT/diode characteristics) must align with operational conditions to ensure reliability.

Limitations of the Study

This study's conclusions are limited by several factors:

Firstly, the findings are based solely on computer simulation (using PLECS) and have not been confirmed with a physical model. That is, real-world issues, such as electrical interference, measurement errors, heat transfer between components and manufacturing variations in parts, were not considered.

Secondly, the simulation's heat model is a simplification based on manufacturer data. It does not capture the complex, 3D manner in which heat actually spreads or changes over time, nor does it

factor in how airflow and surrounding temperature changes will affect performance in a real application.

Thirdly, this research only examines a standard and basic converter design with simple controls. It does not explore how more advanced designs or smarter control methods can change the results. Finally, this investigation was narrow, focusing only on a single specific type of transistor (IKWH70N65WR6 IGBT) and its diode.

The results may not be generalised to other IGBT generations, SiC/GaN devices or different diode technologies with superior reverse recovery characteristics.

Future Work

Future research directions:

- Developing advanced control algorithms and adaptive gate-drive techniques to minimise losses and improve dynamic performance in boost DC– DC converters for PV systems.
- Exploring innovative thermal management strategies to address the challenges posed by high-frequency operation and varying load conditions.

Acknowledgements

We extend our heartfelt gratitude and deepest appreciation to Al-Qadisiyah University, particularly the Department of Electronics and Communication, for their unwavering support, guidance and resources throughout this endeavour.

6. References

- [1] TWIDELL, John. Renewable energy resources., Second edition,: Taylor&Francis, 2021.
- [2] M. D. Almawlawe, M. Al-Badri, and E. J. Alshebaney, "Implementation and evaluation of low switching losses converter for solar panel using digital controller," *AIP Conference Proceedings*, vol. 2797, 2023, p. 050009-1-050009-10, doi: 10.1063/5.0148147.
- [3] T. Esram and P. L. Chapman, "Comparison of photovoltaic array maximum power point tracking techniques," IEEE Transactions on Energy Conversion, vol. 22, no. 2, pp. 439–449, Jun. 2007, doi: 10.1109/tec.2006.874230.
- [4] P. Singh, D. K. Palwalia, A. Gupta, and P. Kumar, "Comparison of photovoltaic array maximum power point tracking techniques,"

- Int. Adv. Res. J. Sci. Eng. Technol, vol. 2, no. 1, pp. 401–404, 2015.
- [5] M. Hawsawi, H. M. D. Habbi, E. Alhawsawi, M. Yahya, and M. A. Zohdy, "Conventional and switched capacitor boost converters for solar PV integration: dynamic MPPT enhancement and performance evaluation," Designs, vol. 7, no. 5, p. 114, Sep. 2023, doi: 10.3390/designs7050114.
- [6] F. L. Luo and H. Ye, Essential Dc/Dc converters., CRC Press, 2018. doi: 10.1201/9781420037104.
- [7] S. S. Ahmad, C. Urabinahatti, K. N. V. Prasad, and G. Narayanan, "High-Switching-Frequency SIC Power Converter for High-Speed Switched Reluctance Machine," IEEE Transactions on Industry Applications, vol. 57, no. 6, pp. 6069–6082, Sep. 2021, doi: 10.1109/tia.2021.3111540.
- [8] Reali, Alessandro., Design of highperformance electronic power converters based on GaN-on-Si semiconductors devices." (2025).
- [9] A. Chaithanakulwat, "Technique Reducing Power Loss in Three-Level DC-DC Converter Devices with Zero-Voltage and zero-Current Switching Method," Journal of Engineering Science and Technology Review, vol. 13, no. 4, pp. 124–131, Aug. 2020, doi: 10.25103/jestr.134.12.
- [10] S. M. I. Rahman *et al.*, "Emerging Trends and Challenges in thermal Management of Power Electronic Converters: A State of the art review," IEEE Access, vol. 12, pp. 50633–50672, Jan. 2024, doi: 10.1109/access.2024.3385429.
- [11] C. R. Sullivan and R. Y. Zhang, "Simplified design method for litz wire," *In 2014 IEEE Applied Power Electronics Conference and Exposition-APEC 2014*, 2014, pp. 2667–2674, doi: 10.1109/apec.2014.6803681.
- [12] W. G. Hurley and W. H. Wölfle, Transformers and Inductors for Power Electronics: Theory, design and Applications.,:John Wiely& Sons, 2013. doi: 10.1002/9781118544648.
- [13] S. C. Trujillo, J. E. Candelo-Becerra, and F. E. Hoyos, "Numerical Validation of a Boost Converter Controlled by a Quasi-Sliding Mode Control Technique with Bifurcation Diagrams," Symmetry, vol. 14, no. 4, p. 694, Mar. 2022, doi: 10.3390/sym14040694.
- [14] N. B.-R. Lin and N. C.-L. Huang, "Interleaved ZVS converter with Ripple-Current cancellation," IEEE Transactions on Industrial Electronics, vol. 55, no. 4, pp.

- 1576–1585, Apr. 2008, doi: 10.1109/tie.2008.917069.
- [15] T. Pei, H. Zhang, W. Hua, and F. Zhang, "Comprehensive Review of Bearing Currents in Electrical Machines: Mechanisms, impacts, and mitigation techniques," Energies, vol. 18, no. 3, p. 517, Jan. 2025, doi: 10.3390/en18030517.
- [16] J. Yang, "Efficiency Improvement with GaN-Based SSFET as Synchronous Rectifier in PFC Boost Converter," PCIM Europe 2014; International Exhibition and Conference for Power Electronics, Intelligent Motion, Renewable Energy and Energy Management; Proceedings .VDE, May 2014, pp. 1–6, [Online].
 - Available: http://ieeexplore.ieee.org/xpls/abs_a ll.jsp?arnumber=6841334.
- [17] M. Almawlawe, H. Hamed, I. Al-Umari, and M. Wali, "Enhanced voltage conversion and reduced inductor size in a flying capacitor boost converter compared to conventional boost converter for photovoltaic systems," Al-Qadisiyah Journal for Engineering Sciences, vol. 17, no. 4, pp. 322–330, Dec. 2024, doi: 10.30772/qjes.2024.152779.1354.
- [18] Y.-W. Cho, J.-M. Kwon, and B.-H. Kwon, "Single Power-Conversion AC--DC converter with high power factor and high efficiency," IEEE Transactions on Power Electronics, vol. 29, no. 9, pp. 4797–4806, Nov. 2013, doi: 10.1109/tpel.2013.2286832.
- [19] W. Hassan, D. Lu, and W. Xiao, "Optimal Analysis and Design of DC-DC Converter to Achieve High Voltage Conversion Gain and High Efficiency for Renewable Energy Systems," IEEE Transactions Power Electronics, Art. no. IEEE Transactions on Power Electronics, 2018 **IEEE** 27th International Symposium on Industrial Electronics (ISIE, Jun. 2018, doi: 10.1109/isie.2018.8433857.
- [20] Q. Liu, A. Ali, and A. Alkhayyat, "Genetic Algorithm-Optimized Convolutional Neural Network Controller for enhanced performance of boost DC-DC converters," vol. 20, no. 8, pp. 5315–5331, Jun. 2025, doi: 10.1007/s42835-025-02315-1.
- [21] Z. H. Al-Araji, M. D. H. Almawlawe, and M. H. Wali, "Comprehensive characterization of switching and conduction losses in high-ratio step-down converters for next-generation electric vehicles," Sustainable Engineering and Innovation, vol. 7, no. 2, pp. 449–462, 2025. doi: 10.37868/sei.v7i2.id633.

تحليل تأثير خسائر التبديل والتوصيل على أداء IGBT في مغيرات التيار المستمر الرافعه المستخدمه في ألأنظمة الكهروضوئية.

مهند ضياء هاشم المولوي

قسم الالكترونيك والاتصالات، كلية الهندسة، جامعة القادسية، القادسية، العراق البريد الالكتروني: muhanad.almawlawe@qu.edu.iq

المستخلص

تبحث هذه الدراسة في تأثير خسائر التبديل والتوصيل على أداء الترانزستورات ثنائية القطب ذات البوابة المعزولة (IGBTs)داخل محولات التيار المستمر التصعيدية ، المصممة خصيصا للأنظمة الكهروضوئية (PV) . يفحص البحث السلوك الحراري ل IGBTs في ظل ظروف تشغيل مختلفة ، بما في ذلك مقاومة الحمل المختلفة (Ω 5 و Ω 10 و Ω 20) ، وترددات التبديل تتراوح من 1كيلو هرتز إلى 100كيلو هرتز ، ومعلمات الإدخال /الإخراج .يتم تحليل المقاييس الرئيسية مثل درجة حرارة المشتت الحراري ودرجة حرارة تقاطع الصمام الثنائي ودرجة حرارة تقاطع IGBT وخسائر اللطاقة لتوفير فهم شامل لمقايضات الكفاءة . تشير النتائج إلى أن خسائر التوصيل تهيمن على الترددات المنخفضة وتيارات الحمل الأعلى ، بينما تصبح خسائر التبديل أكثر وضوحا عند الترددات الأعلى . يظهر التحكم الحراري كعامل حاسم ، حيث تصل درجات الحرارة إلى ذروتها عند ترددات متوسطة المدى (60-50)كيلو هرتز قبل أن تنخفض عند الترددات العالية جدا .بالإضافة إلى ذلك ، تؤدي قيم المقاومة المنخفضة إلى زيادة استهلاك الطاقة والخسائر ، مما يسلط الضوء على هرتز قبل أن تنخفض عند الترددات العالية جدا .بالإضافة إلى ذلك ، تؤدي قيم المقاومة المنخفضة إلى زيادة استهلاك الطاقة والخسائر ، مما يسلط الضوء على أن تنخفض عند الترددات العالية جدا .بالإضافة إلى ذلك ، تؤدي قيم المقاومة المنخفضة إلى زيادة السحث إرشادات مهمة لاختيار وتحسين أداء المحلة والموثوقية في تطبيقات الطاقة المتجددة . ستركز الأبحاث المستقبلية على خوارزميات التحكم المتقدمة وتقنيات محرك البوابة التكيفية لتقليل الخسائر وتعزيز الأداء الديناميكي في محولات التيار المستمر التصعيديه والمستخدمه في منظومات الطاقه الشمسيه.